Density functional theory study on the electronic structures and spectral properties of 3,5-Dimethylanisole dye sensitizer for solar cell applications

Anuradha Mathiyalagan [a],[*], Karnan Manimaran [a], Karunanidhi Muthu [a], Meenakshi Rajakantham [b]

[a] PG & Research Department of Physics, Srimad Andavan Arts and Science College (A), Trichy, Tamilnadu, India
[b] Department of Physics, Cauvery College for Women (A), Trichy, Tamilnadu, India

ARTICLE INFO

ABSTRACT

This paper provides a combination of experimental and theoretical work on the molecular structure and vibrational analysis of 3,5-Dimethyanisole (3,5-DMA). The FT-IR and FT-Raman spectra of the 3,5-DMA compound in the solid phase were observed in the 4000–400 cm^{-1} and 4000–100 cm^{-1} ranges, respectively. The structural and spectroscopic data of the molecules in the ground state were analyzed using Density Functional Theory Methods (DFT) employing B3LYP with 6–31 + G (d,p) and cc-pVTZ basis sets. DFT (B3LYP/6–31 + G (d, p) calculations were used to yield energy, optimize structures, harmonic vibrational frequencies, IR intensities, and Raman activities. Related to the theoretical analysis of 3,5-Dimethylanisole based donor-pi-acceptor (D-PI-A) dyes using time-dependent approaches, where the donor is benzene, triphenylamine (TPA) and the electron acceptor is CN, COOH, NO_2. The HOMO-LUMO analysis is used to calculate the energy gap, ionization potential, electron affinity, global hardness, and chemical potential. Charge distribution analysis, Thermodynamic and magnetic properties are some of the characteristics that can be found for the title compound. Furthermore, electronic spectra and Non-Linear Optical (NLO) properties of 3,5-DMA and its dyes are simulated.

1. Introduction

Anisole is a solvent that has been processed successfully in organic/polymer solar cells. The belongings of anisole C_6H_5-O-CH_3, and its products have been the focused on numerous experimental and theoretical researches on the dye sensitized solar cell applications [1]. The position of the O-CH_3 bond, in the ring plane or perpendicular to it, depends mainly on the equilibrium between conjugations, which suggests a planar structure. Methyl anisole are worthy models to study the methyl internal rotation. These interactions will result in some changes on the geometric structure, vibrations and electronic states of these molecules. The principle aim of this paper is to study the changes in the electronic structure of 3, 5-DMA dyes caused by the introduction of substituents. The Organic pi-conjugate systems represent a new class of materials that can be used in organic electronics.

In DSSC, the dye sensitizer is one of the main components for higher power incident to photon power conversion efficiencies (IPCE). As a key part in DSSCs, the dye sensitizer absorbs the light to inject the excited state of the electron into the semiconductor conduction band edge. A feasible dye must be energy-matched with the semiconductor materials and redox electrolyte. Also, better light harvesting capability along with chemical stability is required for an efficient dye sensitizers [2].

Dye Sensitized Solar Cells (DSSC) have piqued the interest of academic and industry circles due to their outstanding performance and inexpensive cost. Improvements in solar energy to electricity conversion efficiency have remained a major focus of DSSC research. The electrical structure of organic dyes utilised in DSSC was studied using TDDFT simulations.

TDDFT methods were utilised to form a variety of different metal-free organic dye compounds using anisole based on the D-PI-A architecture. This research emphasises the use of benzene and triphenylamine as donors and CN, COOH, and NO_2 as acceptors in DSSC applications, as well as a 3,5-DMA linker as a pi-bridge. Six types of dye structures are designed based on the effective photo induced intramolecular charge-transfer capabilities of the distinct donor, acceptor combinations.

A theoretical calculation approach is an effective tool for the molecular design, and the conclusions generated from the calculations are valuable information for the synthesis of newer efficient dyes. Although

the computed results cannot provide measurable information about dye presentation, the theoretical technique could be a valuable and low-cost tool for molecular design and the selection of more efficient dyes. The synthesis of the acceptor unit in the molecular designing of D-PI-A sensitizers, which would be provided as tuning structures, which is crucial for novel enhancement in obtaining greater Incident Photon to Current Conversion efficiency (IPCE).

For DSSCs, computational investigations were widely applied [3–5]. Density functional theory (DFT) and time-dependent density functional theory (TD-DFT) are used to investigate the geometries, electronic structures, and absorption spectra of dyes 1 to 6, to identify possible dye sensitizers for use of DSSCs. Later, the dye 1 to dye 6 sensitizers' NLO properties were investigated in terms of dipole moment, polarizability, and first-order hyperpolarizability.

2. Results and discussions

2.1. Optimized geometry of 3,5-Dimethylanisole

The optimized structural parameters of the molecule 3,5-DMA are calculated by DFT (B3LYP) with the same basis sets which are listed in Table 1. In accordance with the atom numbering scheme given in Fig. 1. The calculated geometrical parameters represent a good approximation and they are the bases for the calculating other parameter, such as vibrational frequencies, hyperpoalrizability, thermodynamical properties. In all molecules, the assignment of bond type will be unambiguous.
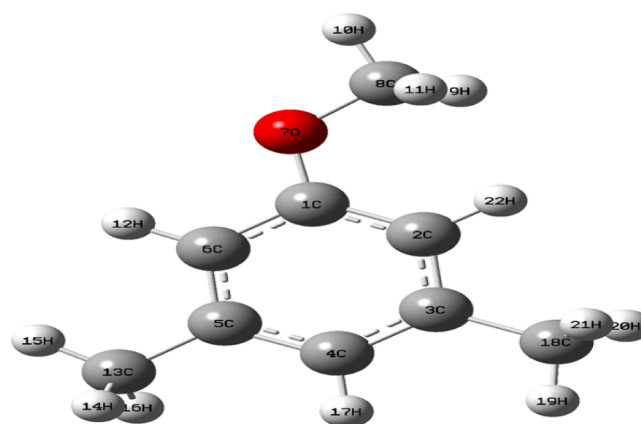

Fig. 1. Optimized structure of 3,5-Dimethylanisole.

Five types of local atomic geometry are distinguished. If the connectivity is 4, tetrahedral angles are used. For connectivity 3, the three bonds are either taken to be planar with bond angles of 120 degree or pyramidal bond angles of 107 degree (the tetrahedral angle). The theoretically designed bond lengths and bond angles are good agreement with the reported [6,7] experimental values and calculated values for relative molecules.

Table 1
Optimized structural parameters of 3,5-Dimehylanisole utilizing B3LYP/6–31 + G(d,P) and B3LYP/cc-pVTZ density functional calculation.

Parameters	Bond Length (Å)		Bond Angle (deg)		Parameters	Dihedral angles (deg)	
	6–31 + G(d,p)	cc-pVTZ	6–31 + G(d,p)	cc-pVTZ		6–31 + G(d,p)	cc-pVTZ
C1-C2	1.396	1.403	120.246	120.219	C6-C1-C2-C3	0.001	0.001
C1-C6	1.405	1.400	124.428	124.153	C6-C1-C2-H22	180.000	180.001
C1-O7	1.370	1.370	115.325	115.628	O7-C1-C2-C3	−180.000	180.000
C2-C3	1.408	1.402	119.863	119.884	O7-C1-C2-H22	−0.001	0.000
C2-H22	1.085	1.088	121.024	120.967	C2-C1-C6-C5	−0.002	0.000
C3-C4	1.394	1.401	119.114	119.149	C2-C1-C6-H12	179.999	180.000
C3-C18	1.513	1.512	119.282	119.294	O7-C1-C6-C5	179.999	−179.999
C4-C5	1.408	1.402	119.610	120.432	O7-C1-C6-H12	0.000	0.001
C4-H17	1.089	1.092	121.108	120.275	C2-C1-O7-C8	−0.008	0.003
C5-C6	1.392	1.399	121.252	121.216	C6-C1-O7-C8	179.991	−179.998
C5-C13	1.513	1.512	119.427	119.398	C1-C2-C3-C4	0.000	−0.002
C6-H12	1.087	1.090	119.321	119.386	C1-C2-C3-C18	179.998	−180.001
O7-C8	1.420	1.422	118.908	118.970	H22-C2-C3-C4	−179.999	179.998
C8-H9	1.098	1.101	120.230	121.012	H22-C2-C3-C18	0.000	−0.001
C8-H10	1.092	1.095	120.863	120.018	C2-C3-C4-C5	−0.001	0.002
C8-H11	1.098	1.101	120.449	120.418	C2-C3-C4-H17	−180.000	−179.999
C13-H14	1.098	1.100	118.403	118.540	C18-C3-C4-C5	−179.999	−179.999
C13-H15	1.095	1.100	121.149	121.042	C18-C3-C4-H17	0.002	0.001
C13-H16	1.098	1.097	118.597	118.326	C2-C3-C18-H19	179.997	120.424
C18-H19	1.095	1.100	111.382	111.378	C2-C3-C18-H20	−59.742	−120.366
C18-H20	1.098	1.100	105.782	105.772	C2-C3-C18-H21	59.735	0.028
C18-H21	1.098	1.097	111.382	111.378	C4-C3-C18-H19	−0.004	−59.576
			109.401	109.380	C4-C3-C18-H20	120.257	59.635
			109.410	109.466	C4-C3-C18-H21	−120.266	180.029
			109.402	109.380	C3-C4-C5-C6	0.000	0.000
			111.224	111.145	C3-C4-C5-C13	179.998	179.999
			111.475	111.145	H17-C4-C5-C6	180.000	180.000
			111.224	111.313	H17-C-C5-C13	−0.003	−0.001
			107.809	107.148	C4-C5-C6-C1	0.001	−0.001
			107.100	107.956	C4-C5-C6-H12	−180.000	−180.000
			107.809	107.956	C13-C5-C6-C1	−179.997	−180.000
			111.351	111.118	C13-C5-C6-H12	0.002	0.001
			111.352	111.118	C4-C5-C13-H14	59.632	120.381
			111.353	111.470	C4-C5-C13-H15	179.988	−120.375
			107.733	107.149	C4-C5-C13-H16	−59.657	0.003
			107.733	107.900	C6-C5-C13-H14	−120.371	−59.620
			107.113	107.899	C6-C5-C13-H15	−0.015	59.624
					C6-C5-C13-H16	120.341	−179.998
					C1-O7-C8-H8	61.235	61.256
					C1-O7-C8-H10	−179.991	179.998
					C1-O7-C8-H11	−61.215	−61.260

2.2. Experimental and Computational details

The samples were obtained from the Sigma Aldrich with a purity of >98 % and it was used as such without additional cleansing. In this study the Fourier Transform Infrared (FT-IR) spectrum of the sample was recorded at room temperature in the region 4000–400 cm^{-1} using Perkin-Elmer spectrum1 spectrophotometer equipped with the composition of the pellet. The BRUKER-RFS 27 spectrometer was used for the Fourier transform Raman (FT-Raman) spectral measurements at room temperature. The sample was packed in a pellet of about 5 mm diameter and excited in the 180° geometry with 1064 nm laser line at 100 MW power from a diode pumped air cooled-cw Nd:YAG laser as an excitation wavelength in the region 4000–0 cm^{-1}.

Using Becke's three parameters and the Lee-Yang-Parr (B3LYP) and

Table 2
Experimental FT-IR, FT-Raman and Calculated DFT-B3LYP/6–31 + G(d,p), DFT B3LYP/ccPVTZ levels of vibrational frequencies (cm^{-1}), IR intensity and Raman intensity (kmmol^{-1}) of 3,5-Dimethylanisole.

No	Observed frequencies (cm^{-1})		Calculated frequencies (cm^{-1})				IR Intensity (kmmol^{-1})		Raman Intensity (kmmol^{-1})		Vibrational assignments
			B3LYP/6–31 + G(d,p)		B3LYP/cc-pVTZ		B3LYP		B3LYP		
	IR	Raman	Unscaled	Scaled	Unscaled	Scaled	6–31 + G(d,p)	cc-pVTZ	6–31 + G(d,p)	cc-pVTZ	
1		3013	3209	3015	3207	3014	10.729	7.780	16.202	16.246	νCH (99)
2	2988		3199	2998	3183	2993	7.797	5.287	24.738	25.148	νCH (99)
3	2952		3170	2956	3164	2945	20.882	15.609	23.898	24.075	νCH (98)
4		2919	3155	2924	3145	2920	26.337	23.222	33.319	33.686	ν_{ass}CH$_3$ (98)
5	2905		3119	2911	3115	2910	21.566	17.077	17.643	17.734	ν_{ass}CH$_3$ (98)
6		2865	3117	2873	3111	2869	19.442	18.469	15.720	15.823	ν_{ass}CH$_3$ (98)
7		2851	3088	2857	3084	2854	19.345	17.178	23.602	23.729	ν_{ass}CH$_3$ (98)
8	2822		3085	2827	3083	2826	20.069	15.210	25.010	25.094	ν_{ass}CH$_3$ (98)
9	2714	2729	3081	2721	3070	2719	41.459	37.089	14.748	14.918	ν_{ass}CH$_3$ (98)
10			3039	2437	3028	2434	31.626	27.819	77.347	78.280	ν_{ss}CH$_3$(99)
11			3037	2219	3026	2213	45.624	39.736	49.762	50.326	ν_{ss}CH$_3$ (98)
12			3023	2067	3006	2069	59.229	56.825	38.114	38.799	ν_{ss}CH$_3$(98)
13	1608	1620	1658	1621	1649	1619	69.340	72.986	12.481	12.615	νCC(70), δCH(23)
14	1596	1593	1644	1598	1635	1591	126.807	124.405	28.030	28.351	νCC(79)
15			1531	1472	1504	1476	14.401	40.999	12.913	13.339	σCH$_3$(70), δCH(13)
16			1527	1468	1502	1471	60.948	50.028	2.399	2.475	σCH$_3$(97)
17	1463		1523	1464	1479	1462	21.684	23.037	9.221	9.719	σCH$_3$(94)
18			1514	1455	1473	1456	8.397	6.986	18.149	19.078	σCH$_3$(90)
19			1509	1451	1464	1448	0.368	4.020	19.457	20.535	σCH$_3$(95)
20		1446	1508	1450	1463	1442	13.543	3.292	7.654	8.081	σCH$_3$(93)
21			1497	1439	1462	1435	2.125	9.101	4.588	4.789	ρCH$_3$(79), δCH(12)
22			1491	1433	1457	1431	4.876	1.491	6.326	6.591	νCC(72), δc-o-cH$_3$(15)
23			1469	1412	1443	1387	18.382	8.627	7.825	8.085	δCH(73), ρCH$_3$(12)
24		1378	1436	1380	1399	1377	0.186	2.475	28.782	30.134	ρCH$_3$(95)
25			1434	1379	1395	1375	0.672	1.456	17.882	18.770	ρCH$_3$(93)
26	1317	1318	1380	1327	1358	1319	59.765	17.535	29.959	30.827	νCC(86), νCO(12)
27	1293	1284	1329	1294	1328	1287	69.772	117.161	12.226	12.250	δCH(87), νCOC(11)
28		1196	1308	1201	1294	1204	27.966	6.787	1.865	1.900	δCH(57), νCC(40)
29			1227	1186	1206	1169	51.621	49.441	3.693	3.802	φCH$_3$(92)
30		1162	1201	1155	1191	1165	42.780	27.835	2.105	2.136	νCCH$_3$(82), νCH(12)
31	1183		1187	1141	1171	1136	46.042	61.540	6.825	6.979	δCH(89), φCH$_3$(7)
32	1159	1139	1179	1133	1158	1137	1.105	0.924	4.238	4.364	φCH$_3$(94)
33	1067	1068	1106	1063	1095	1065	60.043	48.411	3.470	3.528	νCOCH$_3$(68), δCH(18)
34	1043	1041	1071	1047	1048	1008	0.551	0.094	0.425	0.440	φCH$_3$(85)
35			1070	1029	1045	1024	4.618	3.887	0.059	0.061	φCH$_3$(91)
36			1044	1004	1029	999	0.667	2.061	14.151	14.492	φCH$_3$(89)
37	982	986	1026	986	1012	983	1.384	17.443	2.170	2.217	φCH$_3$(91)
38		945	1007	948	1004	947	0.969	1.490	99.405	100.000	δCC(95)
39		911	969	921	970	913	2.858	6.284	0.481	0.480	νCCH$_3$(78),
40	902		938	902	930	904	13.914	6.762	2.545	2.579	νCO(81),
41		842	885	851	879	845	4.830	4.093	1.361	1.376	γCH(93)
42	829	829	860	827	853	826	12.786	4.087	1.495	1.514	γCH(91)
43			843	810	832	800	33.022	35.737	1.725	1.759	γCH(88)
44	688	692	696	696	694	695	9.792	10.041	0.201	0.202	γC C(86)
45	596	582	604	581	598	585	10.070	9.069	31.078	31.564	δCO(92)
46		541	587	549	589	546	1.204	0.863	8.064	8.036	γCO(93)
47		514	546	525	553	512	0.064	0.035	78.949	77.588	γCC(93)
48	504		527	507	534	509	0.006	0.001	3.921	3.848	γCC(91)
49			513	493	511	491	1.599	0.871	26.155	26.323	Ring deformation
50	473	473	484	465	483	464	1.193	1.241	25.316	25.461	δCCH$_3$(87)
51		372	374	360	377	363	1.582	1.848	44.353	43.797	δCOCH$_3$(83)
52		270	276	265	279	269	0.526	0.264	3.141	3.083	τ CH$_3$(97)
53		236	269	239	273	232	0.857	0.857	13.670	13.368	δCCH$_3$(81)
54		216	240	221	230	221	0.321	0.289	53.884	57.954	γCC(91)
55			210	202	213	205	1.744	0.781	36.147	35.334	δCOCH3(87)
56			207	199	212	204	0.939	1.356	61.982	59.746	γOCH3(81),τCH$_3$(15)
57			182	175	183	176	1.238	1.356	1.570	1.560	γCCH$_3$(91)
58			85	82	86	83	5.581	4.664	21.396	20.989	γCOCH3(88)
59			49	47	47	46	0.372	0.247	69.896	74.387	τCH$_3$(89)
60			45	43	45	44	0.024	0.200	100.000	98.449	τCH$_3$(88)

ν-stretching, ν_{ass}- asymmetric stretching,ν_{ss}- symmetrical stretching, δ -in-plane bending, γ-out-of-plane bending, σ-scissoring, ρ-rocking, τ-twisting, φ-wagging

6–31 + G(d) and cc-pVTZ basis sets, the equilibrium ground-state geometries of the title compound and the dyes 1-dyes 6 molecules were investigated using the DFT method [8]. The optimal geometry structures are built without the usage of symmetry restrictions, which are commonly utilised in computational analyses. On the potential energy surfaces, optimised dye structures were also confirmed to be at their minima (no imaginary frequencies). The UV–vis optical absorption parameters were calculated using TD-DFT calculations with the 6–31 + G (d,p) basis set.

2.3. Vibrational analysis

Table 2 shows the observed IR, Raman bands and calculated attribution frequencies. The FT-IR and FT-Raman spectrums of 3,5-DMA are observed and calculated in the Figs. 2a and b, each. The experimental values are in line with those set by B3LYP/ 6–31 + G(d,p) and cc-pVTZ, and theoretical frequency values are therefore discussed.

2.3.1. Vibrations of C—C vibrations

The ring C=C and C—C stretching vibrations, are known as semicircle stretching and usually occurs in the region 1400–1625 cm^{-1} [9]. In this FT-IR and FT-Raman bands occurs at 1608, 1596 and 1620, 1593 cm^{-1} respectively assigned to CC stretching vibrations of 3,5-DMA. The CC in plane vibrations observed at 945 cm^{-1} and CC out of plane bending vibrations appears at 692, 688, 596, 582, 541, 504, 692, 216 cm^{-1} in the IR and Raman spectrum. These assignments are in good agreement with the literature [10,11]. These observed frequencies show that, the substituents in the ring to some extend affect the ring modes of vibrations. The theoretically computed values by B3LYP/ 6–31 + G(d,p) and cc-pVTZ methods are in good agreement with experimental values.

2.3.2. CH$_3$ mode of vibrations

The assignments of methyl group vibration make a significant contribution to the title compound. The investigated molecule under consideration possesses CH$_3$ in third and fifth position of 3,5-DMA in the ring. The CH$_3$ stretching frequencies are expected in the range of 2900–3050 cm^{-1} [11–14]. The asymmetric stretching modes of the methyl group are calculated to be at 2920, 2910, 2869, 2854, 2826 cm^{-1} by B3LYP/ cc-pVTZ method. The bands observe at 2905, 2822, 2919, 2865, 2851 cm^{-1} in the IR and Raman spectrum were assigned as stretching modes of the CH$_3$ group. The rocking modes of the methyl group were calculated to be at 1435, 1377, 1375 cm^{-1} and observed at 1378 cm^{-1} in the IR spectrum.

2.3.3. O-CH$_3$ vibrations

For anisole and its derivatives, the O-CH$_3$ stretching is generally possible in the 1000–1100 cm^{-1} range [15–17]. O-CH$_3$ vibration is found in this compound at 1067, 1068 cm^{-1}. For O-CH$_3$ stretching, the theoretical value for B3LYP/6–31 + G(d,p) and cc-pVTZ coincides with the experimental values of FT-IR and FT-Raman. For anisoles Owen and Hester, bending mode O-CH3 is 310 cm^{-1} [18,19]. The 300–670 cm^{-1} mode for anisole and its derivatives has been proposed by Ramana Rao et al. [16]. In step with the above reference, a band is assigned to the bending mode approximately C—O—CH3 by a theoretically calculated
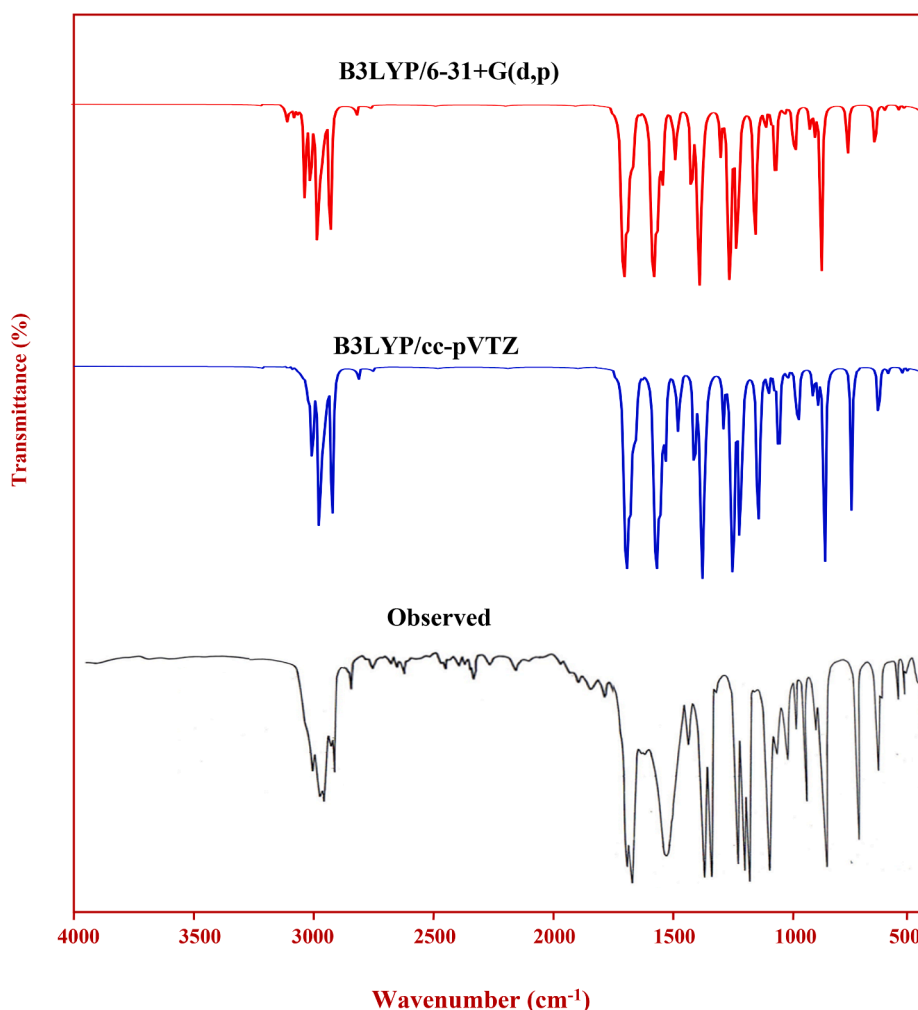

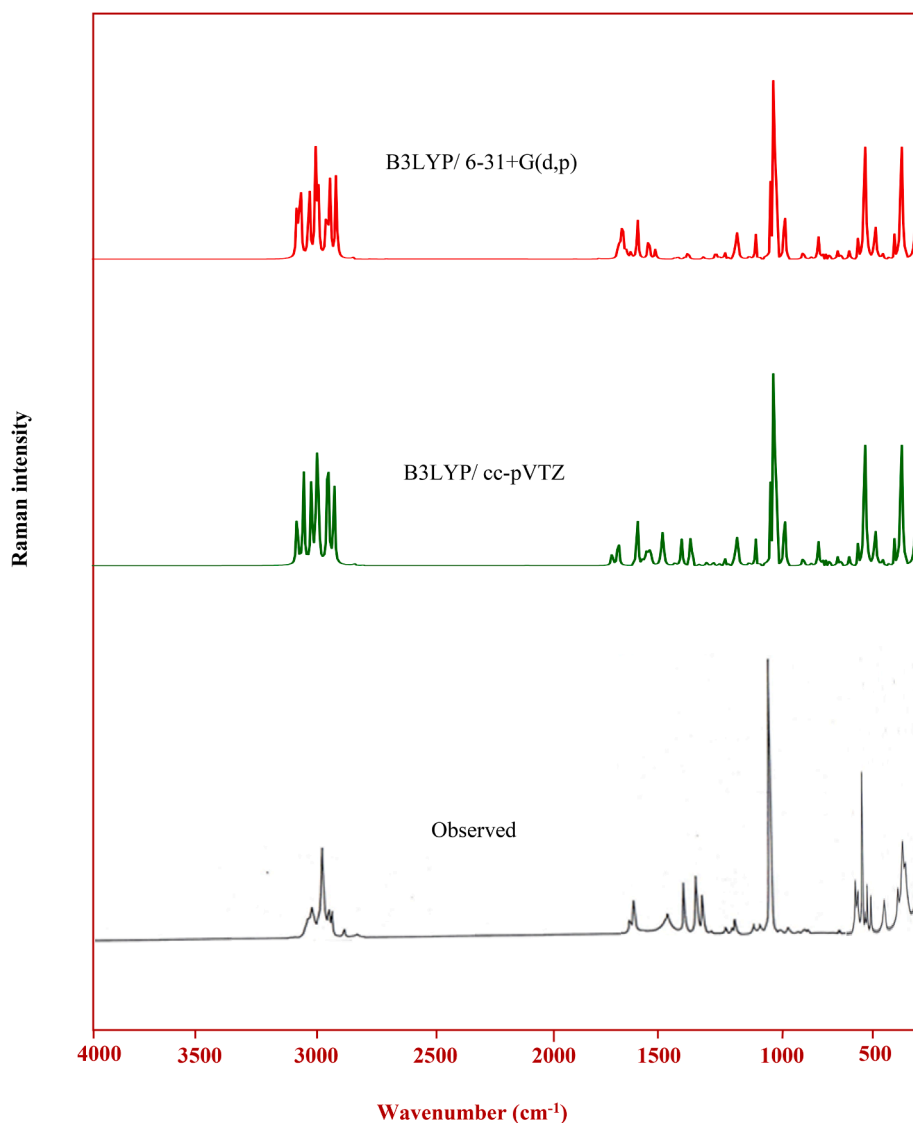**Fig. 2a.** Observed and simulated FT- IR spectra of 3,5-Dimethylanisole.

Fig. 2b. Observed and simulated FT-Raman spectra of 3,5-Dimethylanisole.

value at 360, 363 cm^{-1}.

2.4. Mulliken atomic charge distribution

In the application of quantum mechanical calculations to the molecular systems the computation of atomic charges plays an important role. The charge distributions of the equilibrium geometry of 3,5-Dimethylanisol calculated by the Mulliken [20] are shown in Table 3. The distribution of the charge on the molecule influences vibrational spectrum significantly.

In 3,5-DMA, the Mulliken atomic charge of the C1, C3, C5, C8, C13, C18, H12, H17, H22 become positive, shows the direction of delocalization. The comparison of Mulliken charges obtained by different basis sets are tabulated in Table 3, in order to assess the sensitivity of the calculated charges to change in (i) the choice of the basis set, (ii) the choice of the quantum mechanical method. The results can, however, better be represented in graphical form as shown in Fig. 3.

2.5. Molecular electrostatic potential (MEP)

Molecular electrostatic potential surface of 3,5-Dimethylanisole, which is to locate the positive and negative charged electrostatic potential in the molecule. Colour scale indicates the negative and positive

Table 3
Mulliken population analysis of 3,5-Dimethylanisole performed at B3LYP/ (6–31 + G(d,p) & cc-pVTZ).

Atoms	Atomic charges (a.u)		Atoms	Atomic charges (a.u)	
	B3LYP			B3LYP	
	6–31 + G(d,p)	cc-pVTZ		6–31 + G(d,p)	cc-pVTZ
C1	0.6579	0.6445	H12	0.0424	0.0458
C2	−0.2526	−0.2490	C13	0.0848	0.0797
C3	0.1794	0.1925	H14	−0.0255	−0.0245
C4	−0.2304	−0.2341	H15	−0.0163	−0.0246
C5	0.1975	0.1924	H16	−0.0255	−0.0136
C6	−0.2308	−0.2393	H17	0.0171	0.0206
O7	−0.9019	−0.8772	C18	0.0882	0.0776
C8	0.5376	0.5095	H19	−0.0146	−0.0241
H9	−0.0424	−0.0369	H20	−0.0271	−0.0242
H10	−0.0083	−0.0060	H21	−0.0271	−0.0154
H11	−0.0424	−0.0369	H22	0.0401	0.0432

values. In the Fig. 4 red as negative extreme and blue as positive extreme [21]. The red colour with negative indicates the minimum electrostatic potential that means it is bound loosely or excess electrons present in the surface and act as electrophilic attack. The blue indicate the maximum
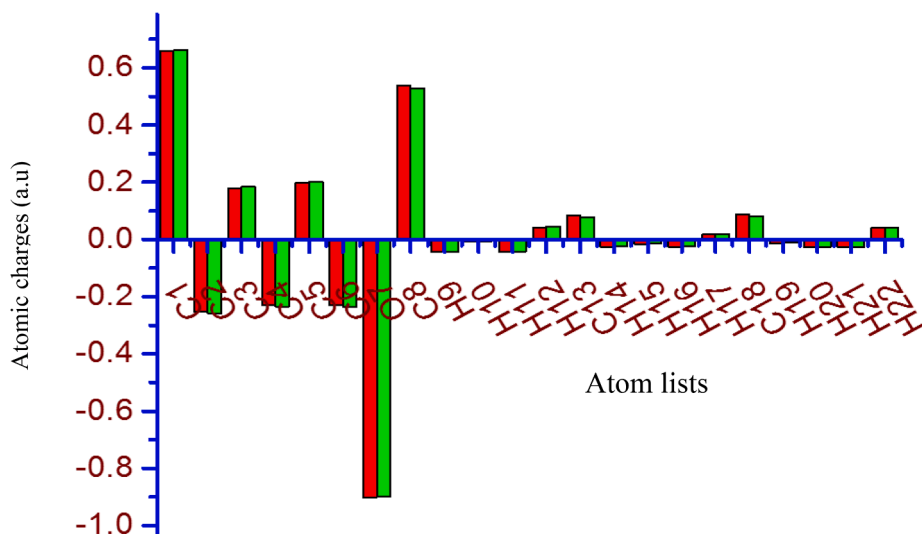
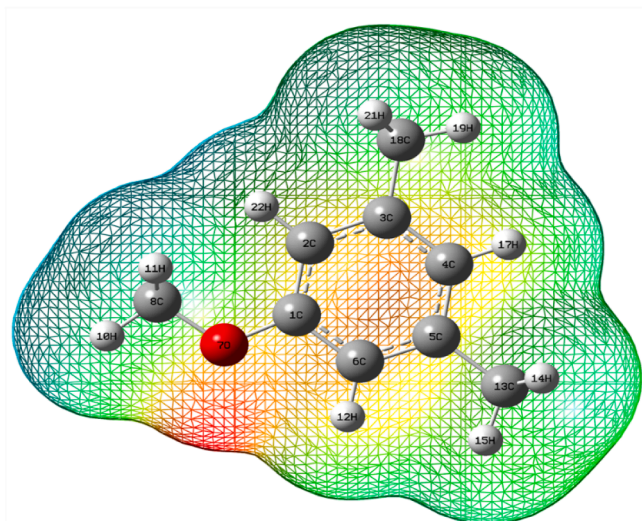**Fig. 3.** Mulliken atomic charge plot of 3,5-Dimethylanisole.

Fig. 4. Molecular electrostatic potential surface of 3,5 -Dimethylanisole.

of electrostatic potential, and it acts opposite [22].

3. Thermodynamical & Magnetic properties

3.1. Thermodynamic functions on the basis of vibrational spectroscopy

The macroscopic state of the thermodynamic system is the theoretical data on molecular structure of 3,5DMA obtained in this work, which allows us to estimate the thermodynamic properties of the title compound. On the basis of vibrational analysis thermodynamic functions Standard entropies (S), heat capacities (C_P), and enthalpies (H), were calculated by statistical thermodynamical formulae. All molecular parameters used in the calculations (Table 4) are obtained by the B3LYP/cc-pVTZ method. Gibbs free energy relates with stability of the molecule, if the energy is small, then the molecule will be at good stability [23,24]. From this, 3,5-DMA has the negative Gibbs free energy. Hence, this result correlates with the Gibbs free energy values, signifying good constancy for the title compound. The relationships between the thermodynamic properties and temperatures were fitted by quadratic equations.

The corresponding fitting equations are as follows and the

Table 4
Statistical thermodynamic parameters of 3,5-Dimethylanisole at various temperatures, performed at B3LYP/cc-pVTZ.

Thermodynamic parameters (k cal/mol)			
Temp. (Kelvin)	Heat capacity (C_P)	Entropy (S)	Enthalpy (H)	Gibbs free energy (G)
50	13.433	62.281	8.667	−53.614
100	19.278	73.134	11.379	−61.756
150	24.645	82.781	15.046	−67.735
200	29.865	92.116	19.325	−72.792
250	35.309	101.370	24.046	−77.325
300	41.003	110.635	29.109	−81.526
350	46.759	119.953	34.449	−85.504
400	52.354	129.348	40.025	−89.323
450	57.631	138.828	45.808	−93.020
500	62.515	148.394	51.776	−96.618

correlation graph is shown in Fig. 5.

Heat capacity (C_P) $= 7.89045 + 0.11189\,X - 3.95909E\text{-}6\,X^2\ R^2 = 0.99979$

Entropy (S) $= 53.1693 + 0.19613\,X - 1.27E\text{-}5\,X^2\ R^2 = 0.99983$

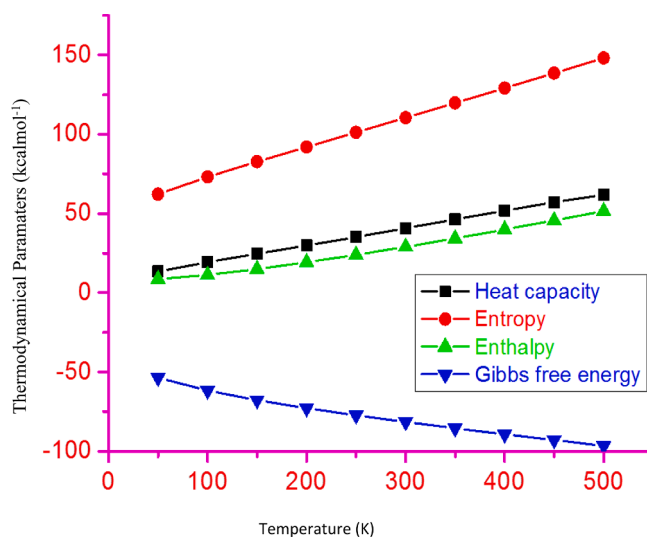Enthalpy (H) $= 5.15412 + 0.05748\,X + 7.27561E\text{-}5\,X^2\ R^2 = 0.99964$

Fig. 5. Thermodynamical properties plot of 3,5-Dimethylanisole.

Gibbs free energy (G) = -48.01543–0.13866 X + 8.54636E-5 X^2 R^2 = 0.99782

3.2. Magnetic moment and Magnetic susceptibility

The number of unpaired electrons provides information about the oxidation state and electron configuration [25]. Magnetic moment is not measured directly. Calculation of moment can give useful chemical information. The value of magnetic moment for oxygen is in Table 5(a). Magnetic moment of the title compound is found to be 2.828 BM. The paramagnetic behaviour of the compounds is due to their incomplete atomic shells. They are all have a critical temperature below which the variation in susceptibility is very different from the variation above it. Any electrons in a 3,5-DMA paramagnetic compounds would have unpaired spins. The Curie plot is a graph about susceptibility vs 1/ temperature. If the Curie-Weiss rule is followed, it should be linear. Since the plot susceptibility vs 1/T for the title compound is linear, the Curie-Weiss rule is followed. This can extract the Curie constant from the slope and the Weiss constant from the x-Intercept from such a plot [26]. Table 5(b) indicates the difference in susceptibility for 3,5-DMA and Fig. 6 shows the Curie plot.

The plot shows that 3,5-DMA is paramagnetic in nature. The following linear equation (regression equation) is considered to be the best fit to predict the value of Curie constant.

Y = −1.22335E−10 + 1.80072 E−5 X R = 0.99999

Curie constant = 0.0000128, Weiss constant = 2.7 × 10^{-08} (BM). The Weiss constant is almost zero. Hence the plot passes through the origin which proves the paramagnetic nature of 3,5-DMA. For the compounds that obey the Curie law, the effective magnetic moment is independent of temperature.

4. Designed dyes structure formation

The chemical structures and labels of different class of dyes are shown in Figs. 7a and b, c. In these structures, a benzene and triphenylamine units are used as the electron-donating moiety and cyano, carboxyl and nitro groups (CN, COOH, and NO_2) were considered as the electron acceptor moiety because of the high electron withdrawing ability and strong bonding to the semiconductor. 3,5-Dimethylanisole used as the π-conjugation system, which bridges the donor–acceptor systems.

To characterize optoelectronic properties, the HOMO, LUMO, and HOMO-LUMO gap (ΔE_{H-L}) of this title compound and its dye 1 to dye 6 are given in Table 6. The plot of frontier molecular orbital analysis is shown in Fig. 8(a). Gauss-sum 2.2 program Boyle et al. [27] were used to calculated group contributions to the molecular orbital (HOMO and LUMO) and prepare the density of states (DOS) spectrum. The DOS spectra were created by convoluting the molecular orbital information with Gaussian curves of unit height. The green and blue line in the DOS spectrum Fig. 8(b) indicated the HOMO and LUMO levels. Here investigated the electron donor effect in the dyes are by using different donor and acceptor groups. In Table 6, 3,5-DMA dye 6 (TPA & NO_2) has the strongest electron donor, acceptor effect. Comparing 3,5-DMA with their dyes, the HOMO energy levels has a tiny change, but the LUMO energy levels of that change obviously. 3,5-DMA dye 2 has the highest HOMO (−5.282 eV).

4.1. Frontier molecular orbital analysis (FMO)

According to the analysis of HOMO in Table 6, results show that the

Table 5a
Magnetic moment of 3,5-Dimethylanisole.

Ions	No. of lone paiirs	Magnetic moment (bohr magnetron)
O	2	2.828

Table 5b
Magnetic Susceptibility of 3,5-Dimethylanisole accomplished at B3LYP/cc-pVTZ.

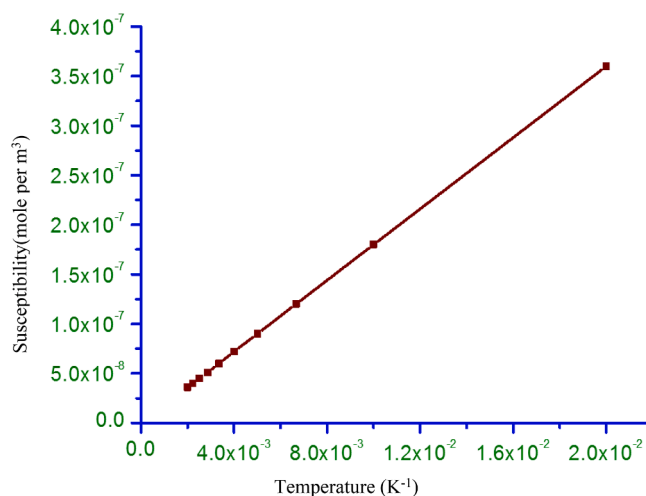| S. No	Temperature (kelvin)	Susceptibility (χ_m) mole per m^3	1/Temp. (Kelvin⁻¹)
1	50	3.6E−07	. 002,000
2	100	1.8E−07	0.01000
3	150	1.2E−07	0.00667
4	200	9.0E−08	0.00500
5	250	7.2E−08	0.00400
6	298.5	6.0E−08	0.00335
7	350	5.1E−08	0.00286
8	400	4.5E−08	0.00250
9	450	4.0E−08	0.00222
10	500	3.6E−08	0.00200

Fig. 6. Magnetic susceptibility plot of 3,5-DMA.

electron-donating ability of dyes 1–6 are in the order 3,5-DMA dye 5 > 3,5-DMA dye 4 > 3,5-DMA dye 6 > 3,5-DMA dye 3 > 3,5-DMA > 3,5-DMA dye 2 > 3,5-DMA dye 1. Dyes 1–3 contain an electron donor moiety as benzene, so that calculated HOMO values are almost in the same range. The molecular orbital energy levels plot for these six dyes are shown in Figs. 9(a) and 9(b). For the D-PI-A dyes, the pi- electron delocalization from the electron donor to the electron acceptor through the pi-conjugated linker 3,5-DMA can affect the performance of the DSSC. So it plays an important role in electron transfer process and photo physical property in the D-PI-A dyes. The calculated energy gap are almost same for 3,5-DMA dye 2 and 3,5-DMA dye 3 which has same donor moiety as benzene and 3,5-DMA dye 6 has the lowest energy gap (3.628 eV). However, in addition to the obvious shift in absolute energy, reveal a clear difference in the energetic ordering of the frontier orbitals in different donor and acceptors.

5. Quantum chemical parameters

5.1. Electrophilies & nucleophilies

The higher HOMO energy corresponds to the more reactive molecule in the reactions with electrophiles. From Table 7 higher HOMO energy corresponds to 3,5-DMA dye 2, which more react with electrophiles. While lower LUMO energy for the dyes 3,5-DMA dye 3 & 3,5-DMA dye 6 is essential for molecular reactions with nucleophiles [28].

5.2. Electronegativity and chemical hardness

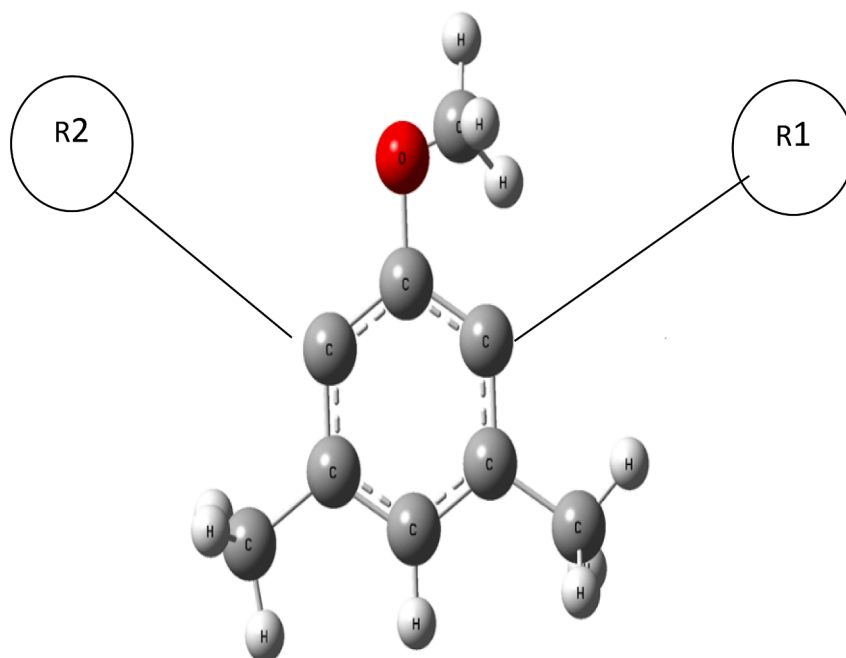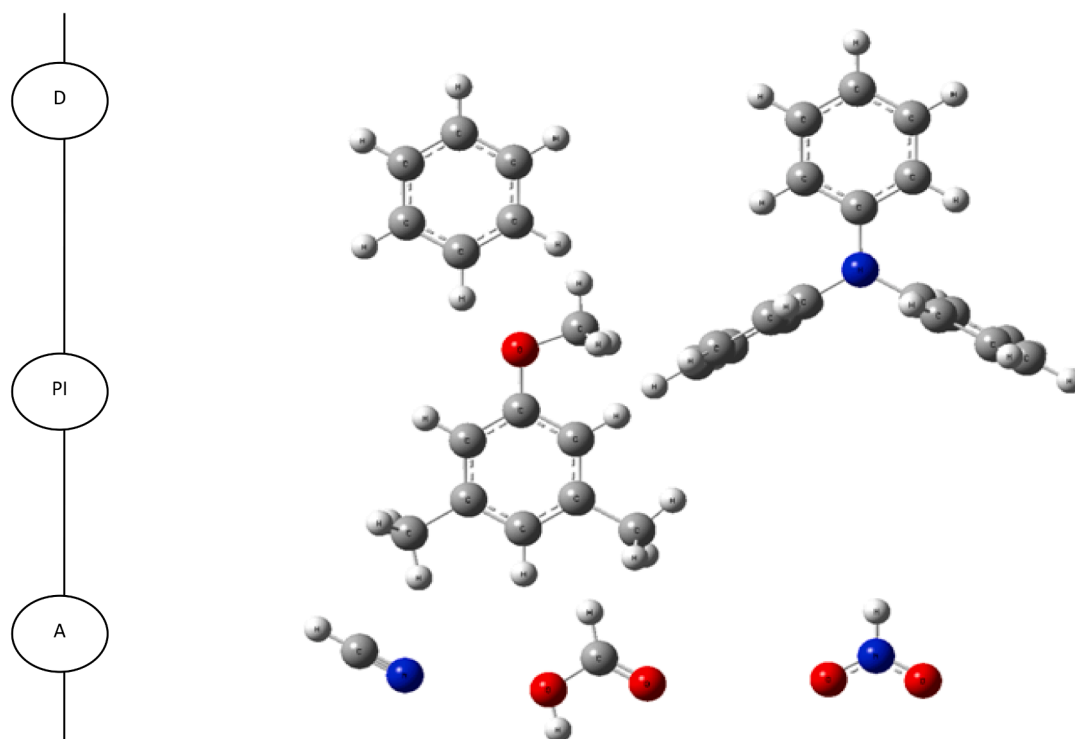The electronegativity, which is the inverse of the chemical potential,

Fig. 7. (a) Different parts of D- π- A system. D = donor, π = pi spacer, A = acceptor 7(b) Chemical Structure of 3,5-Dimethylanisole for newly designed dyes R1 = Benzene, TriphenylamineR2 = CN , COOH, NO$_2$.

is a significant quantum chemistry descriptor for any chemical system's reactivities. To analyze the electronic properties, HOMO and LUMO energy levels between donors and acceptors should be compared. Density functional study (DFT) [29] have been very influential in providing a theoretical framework for common qualitative chemical concepts such as electronegativity (χ), hardness (η), softness (S), and local ones such as the Fukui function F(r) and local softness, S(r).

The fundamental relationship of chemical reactivity in DFT is that it
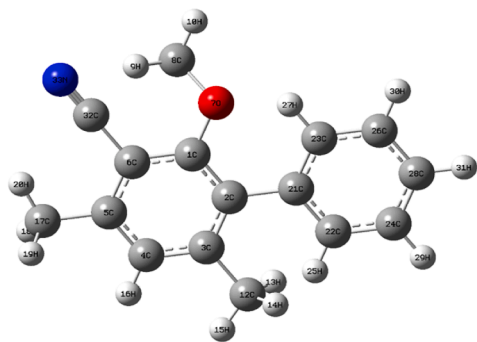
Dye 1 : BENZENE − 3,5-DMA - CN
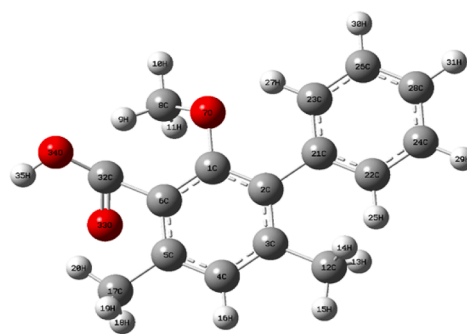
Dye 2 : BENZENE − 3,5-DMA - COOH
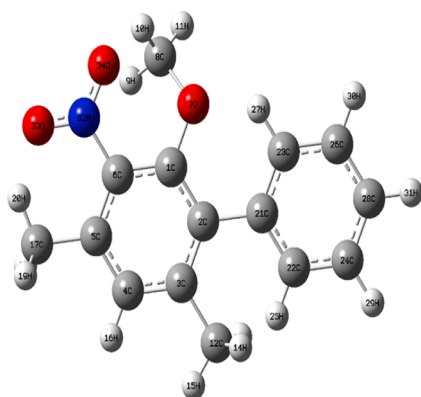
Dye 3 : BENZENE − 3,5-DMA − NO$_2$
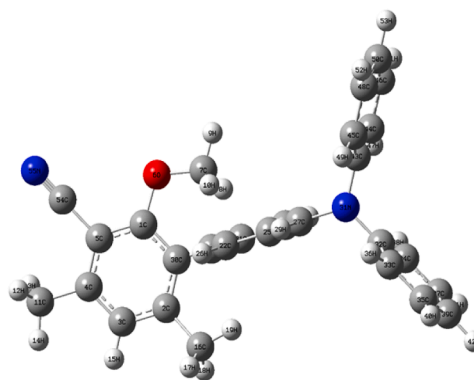
Dye 4 : TPA − 3,5-DMA − CN
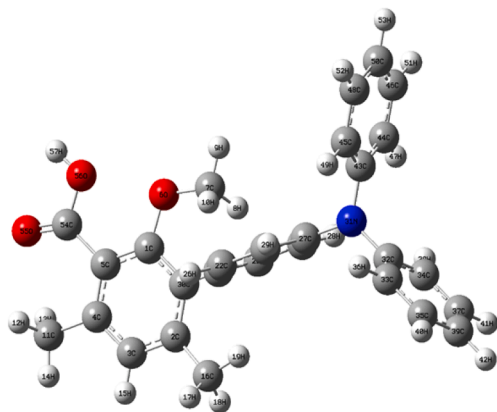
Dye 5 : TPA − 3,5-DMA - COOH
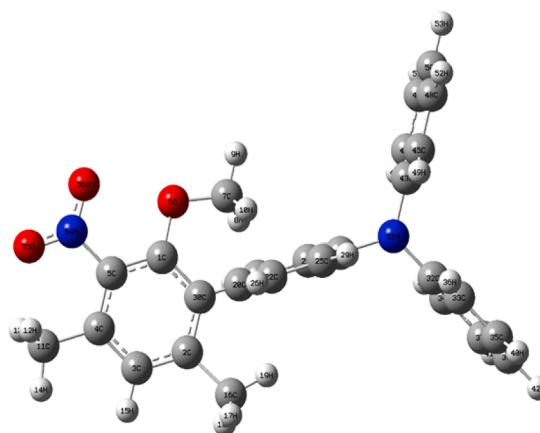
Dye 6 : TPA − 3,5-DMA − NO$_2$

Fig. 7c. Chemical structures of 3,5-Dimethylanisole dyes.

connects the chemical potential of DFT with the energy derivative with respect to the number of electrons, and thus with the negative of electronegativity [30].

$$\mu = \left[\frac{\partial E}{\partial N}\right]_{v(r)} = -\chi; \chi = \frac{IP+EA}{2}$$

where μ is the chemical potential, E is the total energy, N is the number of electrons, and v (r) is the external potential of the system.

Table 6

Frontier molecular orbital analysis of 3,5-Dimethylanisole performed at B3LYP/ 6–31 + G(d,p).

DYES	LUMO Energy (eV)	HOMO Energy (eV)	Energy gap (eV)
3,5DMA	−0.226	− 6.146	5.920
DYE 1	−1.251	− 5.688	4.437
DYE 2	−1.545	−5.282	3.737
DYE 3	−1.962	−5.705	3.743
DYE 4	−1.626	−5.836	4.210
DYE 5	−1.600	−5.617	4.017
DYE 6	−2.204	−5.832	3.628

5.3. Hardness and softness

Hardness (η) has been defined within the DFT as the second order derivative of E with respect to N as v(r) property which measures both the stability and the transport reactivity of the molecule [31–33].

$$\eta = \left[\frac{\partial^2 E}{\partial N^2}\right]_{v(r)} \quad \eta = \frac{IP - EA}{2}$$

where v(r) and μ are, the external and chemical potential respectively.

The Ionization potential (IP) and Electron affinity (EA) of the title compound are calculated using the relation $-E_{HOMO} = IP$, $-E_{LUMO} = EA$. These can predict the transport barrier of the hole and electron in the organic solar cells [34,35]. As shown in Table 7 with the increasing conjugated unit, IP decreased and EA increased. It indicates that the injection ability of hole and electron is improved with the increase of conjugated unit.

The inverse of global hardness (H) is global softness (S) [31]. It assesses the molecular stability and reactivity of a substance. The energy difference between hard and soft molecules is wide in hard molecules and small in soft molecules [36]. Parr [37] proposed the global electrophilicity index, which is equal to $\omega = \mu^2/2\eta$. This index, according to the description, evaluates a chemical species' willingness to accept electrons. 3,5-DMA dye 3 & 6 is a good, more reactive nucleophile with a lower chemical potential and electrophilicity index, while a good electrophile has a high chemical potential and electrophilicity index. The title compound is a strong electrophile when compared to the designed dyes. As the system acquires an additional electronic charge ΔN from the environment, this reactivity index analyses the energy stabilisation.

5.4. Inhibition efficiency

As a function of the inhibitor molecule's reactivity against absorption on the molecular surface, the energy gap is a significant parameter.

HOMO= -6.146 eV   ΔE= 5.920 eV   LUMO=-0.226 eV

Fig. 8a. HOMO, LUMO plot of 3,5-Dimethylanisole.
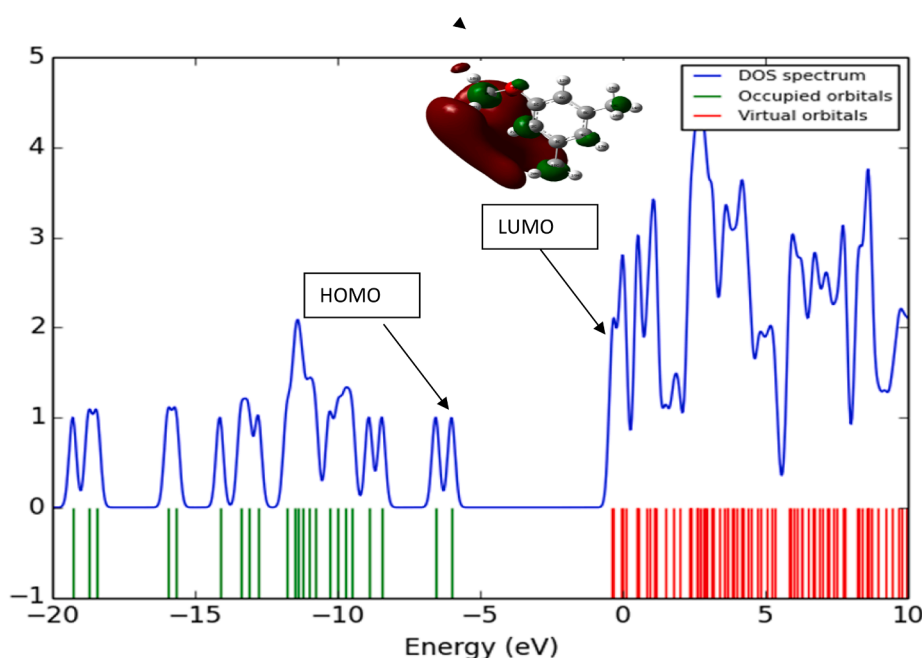
Fig. 8b. Density of states (DOS) diagram for 3,5-Dimethylanisole.

HOMO = -5.688 eV ΔE = 4.437 eV   LUMO = -1.251 eV

HOMO = -5.282 eV ΔE = 3.737 eV   LUMO = -1.542 eV

HOMO = -5.705 eV ΔE = 3.743 eV   LUMO = -1.962 eV
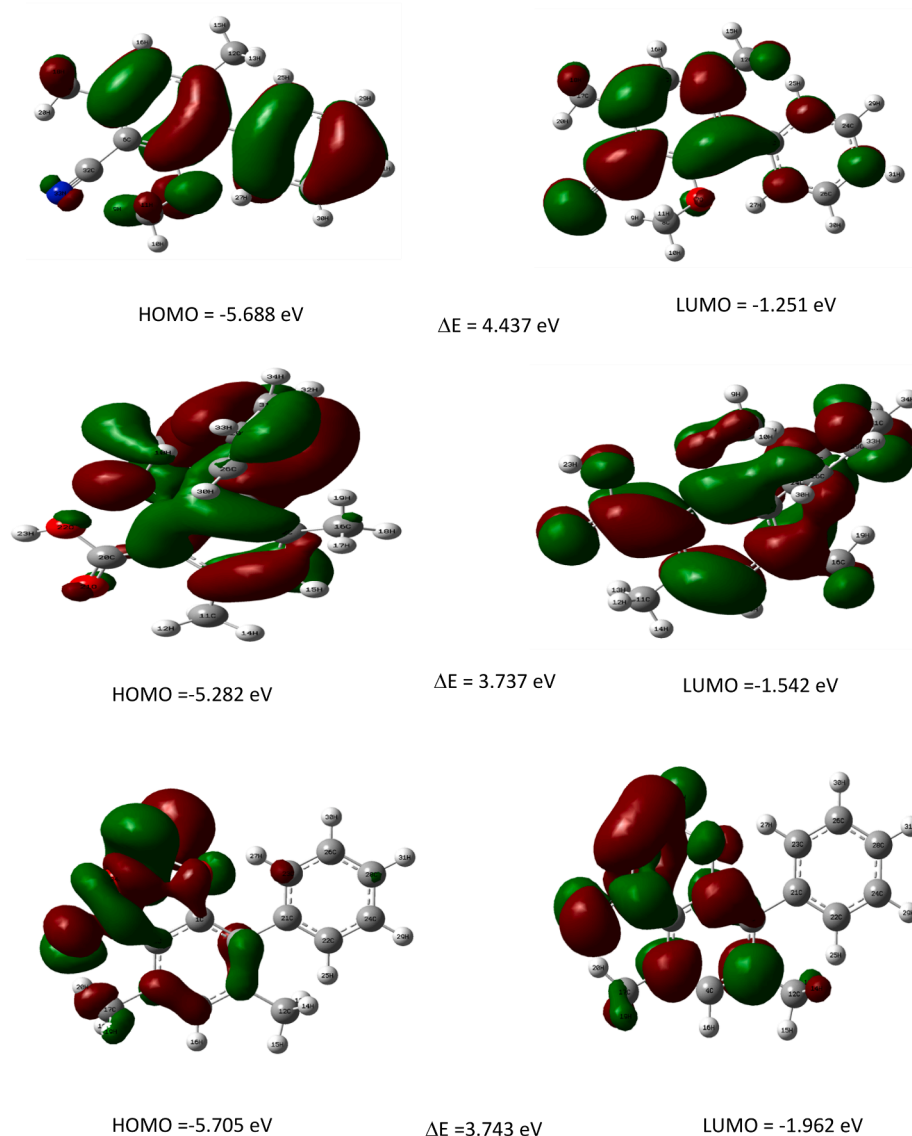
Fig. 9a. Frontier Molecular Orbital analysis of benzene as donor and various acceptors (CN, COOH, NO_2).

If the energy gap narrows, the molecule's reactivity rises, resulting in a rise in the molecule's ionisation potential. Since the energy required to remove an electron from the last occupied orbital is low, a lower value of the energy gap results in good inhibition efficiency [38]. A molecule with low energy gap is more polarizable and associated with the high chemical reactivity and low kinetic stability and is termed soft molecule [39]. The results as indicated in Table 7 shows that inhibitor 3,5-DMA dye 6 has the lowest energy gap, this means that the molecule could have better performance as corrosion inhibitor.

6. Fukui function and local softness

The local selectivity of a corrosion inhibitor is best analysed by means of condensed Fukui function. The change in electron density is the nucleophilic $f^+(r)$ and electrophilic $f^-(r)$ Fukui functions, which can be calculated using the finite difference approximation as follows [30].

$$f_{Ak}^+ = q_{Ak}(N_A + 1) - q_{Ak}(N_A), (\text{for nucleophilic attack})$$

$$f_{Ak}^- = q_{Ak}(N_A) - q_{Ak}(N_A - 1), (\text{for electrophilic attack})$$

$$f_{Ak}^0 = \frac{1}{2}(q_{Ak}(N_A + 1) - q_{Ak}(N_A - 1)), (\text{for radical attack})$$

Where q_{Ak} is the charge of the kth atom in the molecule A, and it can be determined by the use of a Mulliken population analysis [40]. Condensed softness indices which allows the comparison of reactivity between similar atoms of different molecules can be calculated easily starting from the relation between the Fukui function $f(r)$ and the local softness S(r) [41].

$$S(r) = \left[\frac{\partial \rho(r)}{\partial N}\right]_{v(r)} \left[\frac{\partial N}{\partial \mu}\right]_{v(r)} = f(r)S$$

From this relation, one can infer that local softness and Fukui function are closely related, and it plays important role in chemical reactivity.

According to Parr and Yang, a higher value of the Fukui function indicates greater reactivity [42]. As a result, the higher the value of the condensed Fukui function, becomes the more reactive the atomic Center in the molecule is. +(r) denotes the variations in density that occur when a molecule gains electrons, and it correlates to nucleophilic attack reactivity. In contrast, -(r) denoted reactivity in the face of electrophilic attack or when the molecule loses electrons. The Fukui function and
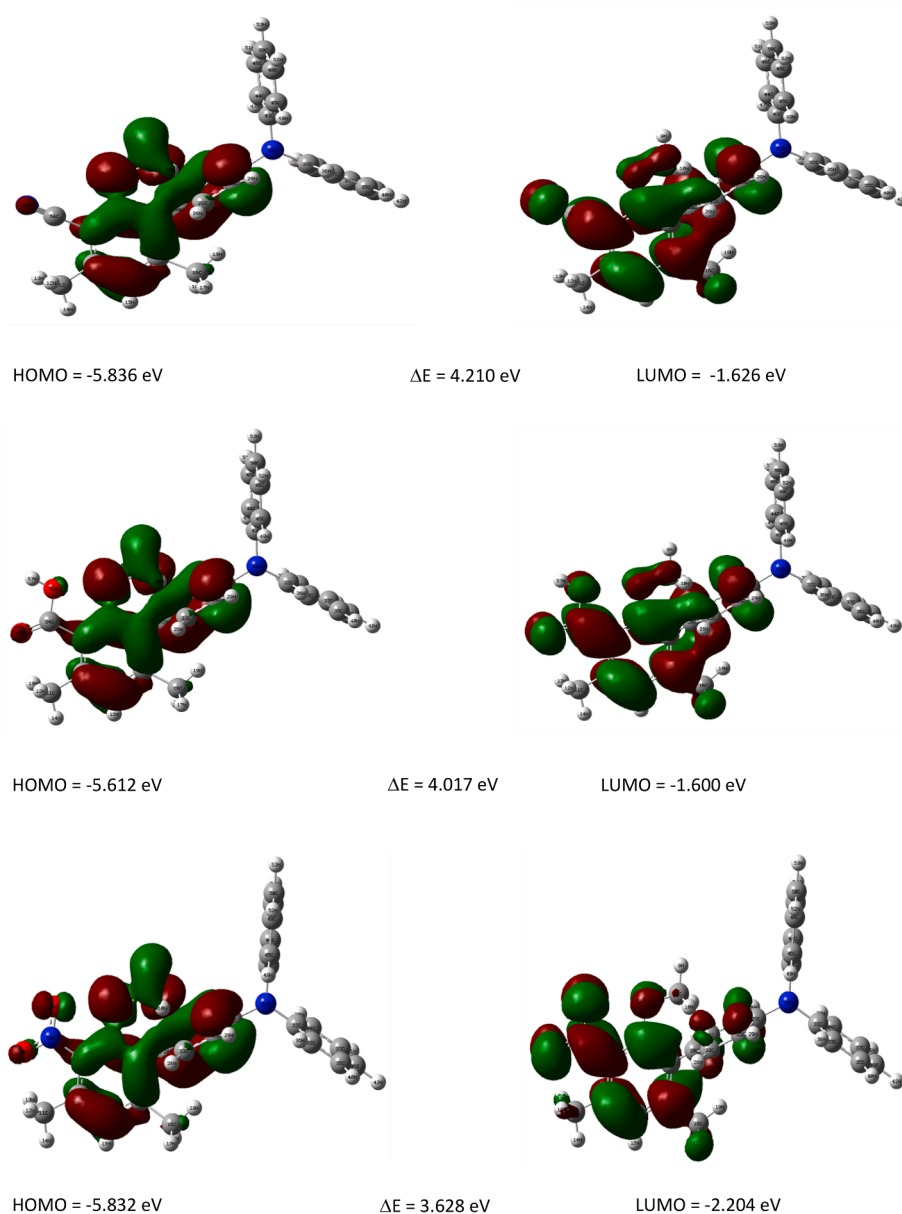
| HOMO = -5.836 eV | ΔE = 4.210 eV | LUMO = -1.626 eV |

| HOMO = -5.612 eV | ΔE = 4.017 eV | LUMO = -1.600 eV |

| HOMO = -5.832 eV | ΔE = 3.628 eV | LUMO = -2.204 eV |

Fig. 9b. 3,5-DMA Frontier Molecular Orbital analysis of TPA as donor and various acceptors (CN,COOH,NO₂).

Table 7

Quantum Chemical Parameters of 3,5-Dimethylanisole calculated B3LYP/ 6–31 + G(d,p) basis set.

Parameters	Values (eV)						
	35DMA	35DMA - DYE1	35DMA - DYE2	35DMA - DYE3	35DMA - DYE4	35DMA - DYE5	35DMA - DYE6
Ionaization Potential (IP)	6.146	5.688	5.282	5.705	5.836	5.617	5.832
Electron Affinity (EA)	0.226	1.251	1.545	1.962	1.626	1.600	2.204
Energy gap	5.920	4.437	3.737	3.743	4.210	4.017	3.628
Hardness(η)	2.960	2.219	1.869	1.871	2.105	2.008	1.814
Softness(S)	0.169	0.225	0.268	0.267	0.238	0.249	0.276
Chemical potential(μ)	−3.186	−3.470	−3.414	−3.834	−3.731	−3.609	−4.018
Electrophilicity index (ω)	1.714	2.713	3.119	3.927	3.307	3.243	4.451
Charge Transfer (ΔN_{max})	1.076	1.564	1.827	2.048	1.773	1.797	2.215
Nucleofugality (ΔEn)	1.940	3.964	4.664	5.889	4.934	4.844	6.655
Electrofugality (ΔEe)	7.860	8.401	8.401	9.632	9.144	8.860	10.283
Back donation(ΔE)	−0.740	−0.555	−0.467	−0.468	−0.526	−0.502	−0.454

local softness are examples of properties that provide details about the various sites within a molecule. It is easier to condense their values around each atomic site into a single value that characterises the atom in the molecule rather than using f(r) or S(r) explicitly. Table 8 shows the values of the simplified Fukui function c for the various systems. In the present case, the electrophilic regions are oxygen atoms and

Table 8
Condensed Fukui functions for 3,5-Dimethylanisole calculated at B3LYP/cc-pVTZ method.

Atom	$q_k(N+1)$	$q_k(N)$	$q_k(N-1)$	f_k^n	f_k^e	f_k^r	Δf_r	s_k^n	s_k^e	s_k^r	ω_k^+	ω_k^-	ω_k°
C1	6.6291	0.6579	0.1368	3.246	0.521	3.246	5.450	2.300	0.201	1.250	19.526	1.704	10.615
C2	−6.0010	−0.2526	0.0387	−3.020	−0.291	−3.020	−5.457	−2.214	−0.112	−1.163	−18.797	−0.952	−9.875
C3	9.2667	0.1794	0.0177	4.625	0.162	4.625	8.926	3.500	0.062	1.781	29.716	0.529	15.122
C4	−11.9989	−0.2304	0.4279	−6.213	−0.658	−6.213	−11.110	−4.532	−0.254	−2.393	−38.483	−2.153	−20.318
C5	7.0667	0.1975	−0.1847	3.626	0.382	3.626	6.487	2.645	0.147	1.396	22.462	1.250	11.856
C6	−2.7796	−0.2308	0.2980	−1.539	−0.529	−1.539	−2.020	−0.982	−0.204	−0.593	−8.335	−1.729	−5.032
O7	−0.0312	−0.9019	0.2705	−0.151	−1.172	−0.151	2.043	0.335	−0.451	−0.058	2.847	−3.834	−0.493
C8	−0.8906	0.5376	−0.0165	−0.437	0.554	−0.437	−1.982	−0.550	0.213	−0.168	−4.670	1.812	−1.429
H9	0.0111	−0.0424	0.0181	−0.003	−0.061	−0.003	0.114	0.021	−0.023	−0.001	0.175	−0.198	−0.011
H10	−0.0059	−0.0083	0.0001	−0.003	−0.008	−0.003	0.011	0.001	−0.003	−0.001	0.008	−0.027	−0.010
H11	0.0113	−0.0424	0.0181	−0.003	−0.060	−0.003	0.114	0.021	−0.023	−0.001	0.176	−0.198	−0.011
H12	0.0015	0.0424	−0.0121	0.007	0.055	0.007	−0.095	−0.016	0.021	0.003	−0.134	0.178	0.022
C13	−1.0661	0.0848	0.0050	−0.536	0.080	−0.536	−1.231	−0.443	0.031	−0.206	−3.764	0.261	−1.751
H14	0.0041	−0.0255	−0.0026	0.003	−0.023	0.003	0.053	0.011	−0.009	0.001	0.097	−0.075	0.011
H15	0.0043	−0.0163	−0.0026	0.003	−0.014	0.003	0.034	0.008	−0.005	0.001	0.067	−0.045	0.011
H16	−0.0006	−0.0255	−0.0005	0.000	−0.025	0.000	0.050	0.010	−0.010	0.000	0.081	−0.082	0.000
H7	−0.0066	0.0171	−0.0171	0.005	0.034	0.005	−0.058	−0.009	0.013	0.002	−0.078	0.112	0.017
C18	0.7889	0.0882	−0.0056	0.397	0.094	0.397	0.607	0.270	0.036	0.153	2.291	0.306	1.299
H19	0.0013	−0.0146	0.0062	−0.002	−0.021	−0.002	0.037	0.006	−0.008	−0.001	0.052	−0.068	−0.008
H20	0.0010	−0.0271	0.0067	−0.003	−0.034	−0.003	0.062	0.011	−0.013	−0.001	0.092	−0.111	−0.009
H21	0.0025	−0.0271	−0.0007	0.002	−0.026	0.002	0.056	0.011	−0.010	0.001	0.097	−0.087	0.005
H22	−0.0080	0.0401	−0.0014	−0.003	0.041	−0.003	−0.090	−0.019	0.016	−0.001	−0.157	0.136	−0.011

nucleophilic regions are mainly CH descriptor, in addition to the information regarding electrophilic/nucleophilic power of a given atomic site is in the molecule, Morell, Toro-Labbe et al., [43] proposed a dual descriptor (Δf(r)), which is defined as the difference between the nucleophilic and electrophilic Fukui function and is given by,

$$\Delta f(r) = [f^+(r) - f^-(r)]$$

Δf(r) > 0, then the site is favoured for a nucleophilic attack, whereas if Δf(r) < 0, then the site may be favoured for an electrophilic attack.

The relativity descriptors, f(r), provide useful information on both stabilising and destabilising interactions between a nucleophile and an electrophile, as well as assisting in the identification of electrophilic/nucleophilic behaviour of a particular site within a molecule. The findings are tabulated in Table 8 and show a positive value for nucleophilic attack and a negative value for electrophilic attack. During a reaction, the behaviour of molecules as electrophiles/nucleophiles is determined by their local behaviour.

7. Nonlinear optical properties

3,5-Dimethylanisole dyes have the highest molecular hyperpolarizability in nonlinear optics due to charge symmetry in the molecules. Information processing, integrated optics, laser doublers, and liquid crystals are all examples of applications for this phenomenon [44]. Wide second-order NLO properties of donor (D) – acceptor (A) substituted organic molecules have been the subject of extensive study. The electrostatic properties of the excited state are crucial for studying materials with nonlinear optical properties [45]. Understanding the structure of the compound for NLO property relationships of D-A molecules is critical for developing strategies to improve NLO response. Zhang et al. [46] investigated the first hyperpolarizability of metal–organic chromophore systems using time-dependent density functional theory and the summation-over-states scheme. The components and final total hyper-polarizabilities for all dyes were calculated after the geometry optimization, as shown in Table 9. The magnitude of the first

Table 9
Nonlinear optical properties of 3,5-Dimethylanisole performed at 6–31 + G(d,p).

Parameters	3,5 DMA		Dye1	Dye 2	Dye 3	Dye 4	Dye 5	Dye 6
	B3LYP							
	6–31 + G(d,p)	cc-pVTZ						
μ_x	0.5446	0.5076	1.2238	−3.6647	1.7176	4.4872	3.7477	4.9746
μ_y	1.1566	1.0185	3.3839	1.1293	2.8324	−4.8915	−1.5264	−4.5366
μ_z	−0.0001	0.0001	0.9145	0.0947	0.4656	0.067	0.1477	0.06
μ_{tot}	1.2784	1.138	3.7128	3.836	3.3451	6.6383	4.0493	6.7328
α_{xx}	−52.6191	−53.4245	−115.424	−118.2381	−120.6412	−206.891	−196.2329	−214.368
α_{yy}	−59.3449	−59.303	−97.6702	−107.1578	−113.225	−186.3546	−171.8481	−187.6837
α_{zz}	−64.5249	−64.2186	−110.9365	−107.8441	−115.908	−168.9362	−191.6273	−172.6618
α_{xy}	3.0129	2.6251	−8.5897	4.0325	−1.1196	32.1782	−9.4616	25.7813
α_{xz}	−0.0005	−0.00053	−1.6188	−0.0045	−0.8898	−0.1858	3.5558	−0.2234
α_{yz}	0.0002	−0.00031	−1.7819	0.3611	−0.3011	−0.7349	−0.5754	−0.7913
$\Delta\alpha(esu)$	−58.8296	−58.9820	−108.0102	−111.08	−113.225	−187.393	−187.9731	−191.5711667
β_{xxx}	31.4265	30.9904	80.7816	−67.658	54.9395	148.8052	135.3038	120.5821
β_{yyy}	−2.5381	−3.1189	5.1008	−23.2479	0.9553	−33.3471	53.2202	−0.8306
β_{zzz}	0.001	0.0011	1.5488	0.8507	−2.7116	−1.2733	−0.6798	−0.4023
β_{xyy}	−2.0761	−2.1897	18.9868	36.7083	1.6218	120.6277	−4.1555	71.5917
β_{xxy}	1.8184	2.2567	54.0813	−20.5497	15.3131	−210.4948	−56.8257	−149.2543
β_{xxz}	−0.0017	−0.0007	5.6553	0.2088	2.5857	−3.8298	−0.3956	−2.864
β_{xzz}	5.0907	4.5632	−13.0847	−3.2729	−26.6232	31.4784	16.5324	8.1858
β_{yzz}	−0.3451	−1.4034	−1.2224	−9.9671	−4.4102	3.3252	9.844	11.2245
β_{YYZ}	−0.0003	−0.0002	5.8544	2.5288	0.4563	1.6785	3.773	2.1297
β_{xyz}	0.001	−0.0002	5.5989	−5.305	3.1659	2.2679	−0.8811	1.7006
$\beta_{tot}(esu)$	2.57284E−30	2.49692E−30	7.84675E−30	4.76624E−30	2.4044E−30	2.87645E−29	1.10385E−29	1.82021E−29

hyperpolarization for 3,5-DMA, 3,5-DMA dye 1, 3,5-DMA dye 2, 3,5-DMA dye 3, 3,5-DMA dye 5, 3,5-DMA dye 6 are substantially lower than the same serial compounds The highest hyperpolarization is seen in 3,5-DMA dye 4 with a donor triphenylamine and acceptor CN, and the maximum first hyperpolarization is seen in 3,5-DMA dye 6 with the same donor (TPA). The relationship between total hyperpolarizabilities and donor or acceptor character has been established: greater hyperpolarizabilities can be attributed to a stronger electronic interaction between donor and acceptor by increasing charge transfer characteristics coupling [47–50].

8. Electronic properties

The electrostatic properties of molecules in their electronically excited states are of considerable interest since they determine many of their observable properties and they contain information on the nature of excited states.

8.1. Optical absorption

TD-DFT calculated absorption spectra has been investigated for title compound and calculated TD-DFT spectra for different dyes with donors as benzene and triphenylamine are displayed in Fig. 10 respectively.

8.2. Open circuit voltage

The short circuit photocurrent density (JSC), open-circuit voltage (VOC), and fill factor (FF), as well as the strength of the incident light (IS), are all closely linked to the power conversion efficiency [51]. The difference between the HOMO of the electron donor and the LUMO of the acceptor PCBM ([6,6]-phenyl-C61butyric acid methyl ester) and TiO_2 determines the open circuit voltage V_{OC}. PCBM is the most broadly used as an acceptor in solar cell applications, this acceptor has the function of accepting the electrons from the donor and thus ensures charge separation [52]. The obtained values are shown in Table 10. It also has an impact on the overall efficiency of power conversion. In the case of TiO_2, the V_{OC} of the studied dyes increases in the following order: 3,5-DMA > 3,5-DMA dye 1 > 3,5-DMA dye 2 > 3,5-DMA dye 5 > 3,5-DMA dye 4 > 3,5-DMA dye 3 > 3,5-DMA dye 6 and from PCBM the calculated values range from (2.7460–1.882 eV). The efficiency of electron injection is improved when dye 6 (C60-OMe) and dye 3 (PCBM) have small values. Exciton binding energy (EBE) is also listed in Table 10.

8.3. Light harvesting efficiency

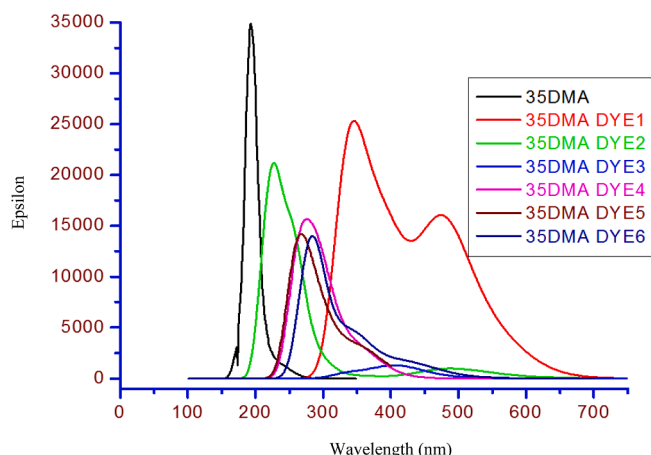The oscillator strength (f) is the added descriptor that converses the

Fig. 10. UV–vis simulated absorption spectra of 3,5- Dimthylanisole.

probability of absorption of electromagnetic radiation by transitions between the energy levels of an atom or molecule [53]. The values of oscillator strength for these dyes at maximum absorption are listed in Table 11, revealing values in the range of 0.1186 to 0.4302. Moreover the oscillator strength, another factor associated with the efficiency of DSSCs is the light harvesting efficiency (LHE). The LHE of 3,5-DMA dye 1 exhibits maximum photocurrent response of absorption wavelength 201 nm. The corresponding absorption thresholds are listed in Table 11.

8.4. Free injection electron energy

For studying photovoltaic efficiency, calculating the electron injection rate from the dye to the TiO2 semiconductor's conduction and dye regeneration by the electrolyte is very useful [54–57]. The free injection electron energy ΔG_{Inject} and ΔG_{Reg} are relevant parameters to consider when examining the relationship between the electronic structure and Jsc. Fast electron transfer generally requires low ΔG_{Inject} and ΔG_{Reg}. The calculated values of these parameters are presented in Table 12. ΔG^{Inject} is negative for all the designed dyes. The calculated values for all dyes increases in the order 3,5-DMA dye 6 > 3,5-DMA dye 2 > 3,5-DMA dye 3 > 3,5-DMA dye 4 > 3,5-DMA dye 1 > 3,5-DMA dye 5 > 3,5-DMA. These results concludes that 3,5-DMA dye 6 which has more positive value, indicating that the excited electron in the dye can escape easily into the conduction band of TiO_2, promoting the injection phenomenon.

9. Conclusion

Detailed vibrational assignments for 3.5-Dimethylanisole are provided and the FT-IR and FT-Raman are registered. The thermodynamic function was obtained by statistical method and magnetic susceptibility from spectroscopic data. The calculations of the correlation between the computational and molecular-electronic 3,5-Dimethylanisole structure parameters and their dyes are calculated using the TD-DFT B3LYP/ 6–31 + G(d,p) basis set. It is theoretically discussed that there are a 3,5-Dimethylanisole-based dyes series that contain various donors and accepters for high performance DSSCs. All of the dyes are designed and discussed in terms of their geometrical, electronic structure, optical absorption properties, and frontier molecular orbitals. With the aim of identifying sensitizers with potential for use in DSSCs, photovoltaic properties such as open circuit voltage, light harvesting efficiency, and electron injection efficiency are discussed in addition to electronic properties. These dyes, especially 3,5-Dimethylanisole dye 6 with TPA as donor and NO_2 as acceptor, have good optoelectronic properties for use in DSSCs, according to the findings. The absorption spectra of dye 1 to dye 6 indicates enhanced red shifts compared to 3,5-Dimethylanisole. Due to its small energy gap, improved optical properties, and sufficient FMO energy levels, this was discovered to be the best photosensitizer. As compared to the other dyes tested, this was found to be the best photosensitizer due to its narrow energy gap, better optical properties, acceptable FMO energy levels, and higher ΔG^{Inject} and ΔG^{Reg} values. The addition of the photon has a major impact on all NLO properties of 3,5−Dimethylanisole molecules. These characteristics make 3,5-Dimethylanisole derivatives a promising photonics candidate. Different electron side groups were also added to see what impact they had on the electronic structure. The computed results of this work may be useful for the enhancement of efficient sensitizers with desirable optoelectronic properties.

Table 10

Energy values of E_{LUMO} (eV), E_{HOMO} (eV), and the open circuit voltage Voc (eV) of 3,5-Dimethylanisole and its dyes.

Dyes	E_{HOMO} (eV)	E_{LUMO} (eV)	V_{oc}(eV)/PCBM	V_{oc}(eV)/Tio$_2$	α_I(eV)	EBE (eV)
3,5-dma	−6.146	−0.226	2.7460	3.774	−3.474	−0.402
Dye 1	−5.688	−1.251	2.2882	2.749	−2.449	−1.727
Dye 2	−5.282	−1.545	1.8820	2.455	−2.155	−1.016
Dye 3	−5.705	−1.962	2.3075	2.037	−1.737	−1.899
Dye 4	−5.836	−1.626	2.4360	2.374	−2.074	−0.066
Dye 5	−5.617	−1.601	2.2170	2.399	−2.099	−0.212
Dye 6	−5.832	−2.204	2.4320	1.796	−1.496	−0.644

Table 11

Light harvesting efficiency (LHE) of 3,5-Dimethylanisole and its derivatives calculated using TD-DFT/B3LYP/6–31 + G(d,p) basis set.

Dyes	Wavelength (nm)	Excitation energy (eV)	Oscillator strength	LHE
3,5-DMA	196	6.3220	0.3850	0.5879
Dye 1	201	6.1643	0.4302	0.6286
Dye 2	261	4.7534	0.1951	0.3619
Dye 3	258	4.7990	0.2363	0.4196
Dye 4	290	4.2761	0.1686	0.3217
Dye 5	293	4.2290	0.1428	0.2802
Dye 6	290	4.2715	0.1186	0.2390

Table 12

Electron injection efficiency of 3,5-Dimethylanisole and its dyes 1 to 6.

Dyes	E_{ox}^{dye}(eV)	E_{ox}^{dye*}(eV)	λmaxICT(eV)	ΔG^{inject}	ΔG^{Reg}
3,5-DMA	6.146	1.060	5.086	−2.950	−1.346
Dye 1	5.688	1.992	3.696	−2.018	−0.888
Dye 2	5.282	2.745	2.537	−1.265	−0.482
Dye 3	5.708	2.676	3.032	−1.334	−0.908
Dye 4	5.836	2.379	3.457	−1.631	−1.036
Dye 5	5.167	1.884	3.283	−2.126	−0.367
Dye 6	5.832	2.915	2.917	−1.095	−1.032

Declaration of Competing Interest

The authors declare that they have no known competing financial interests or personal relationships that could have appeared to influence the work reported in this paper.

References

[1] S. Venkatesan, Q. Chen, E.C. Ngo, N. Adhikari, K. Nelson, et al., Wiley online lib. 2 (2014) 269–274.
[2] H. Zhu, W. Li, Y. Wu, B. Liu, S. Zhu, X. Li, H. Ågren, W. Zhu, Insight into Benzothiadiazole acceptor in D-A–π–A configuration on photovoltaic performances of dye-sensitized solar cells, ACS Sustain. Chem. Eng. 2 (2014) 1026–1034.
[3] W.R. Duncan, O.V. Prezhdo, Theoretical studies of photoin- duced electron transfer in dye-sensitized TiO2, Ann. Rev. Phys. Chem. 58 (2007) 143–184.
[4] P. Li, Y. Cui, C. Song, H. Zhang, A systematic study of phenoxazine-based organic sensitizers for solar cells, Dyes Pigments 137 (2017) 12–23.
[5] C.C. Chiu, Y.C. Sheng, W.J. Lin, R. Juwita, C.J. Tan, H.H.G. Tsai, Effects of internal electron-withdrawing moieties in D-A-π-A or- ganic sensitizers on photophysical properties for DSSCs: A compu- tational study, ACS Omega 3 (2018) 433–445.
[6] W.B. Tzeng, K. Narayanan, J.L. Lin, C.C. Tung, Spectrochim. Acta 55A (1999) 153–162.
[7] S.A. Katsyuba, R. Schmutzler, U. Hohm, C. Kunze, J. Mol. Struct. 610 (2002) 113–125.
[8] H.M. Seip, R. Seip, Acta Chem. Scand. 27 (1973) 4024–4027.
[9] K. Ohno, H. Abe, S. Masatoki, H. Yoshida, H. Matsuura, J. Phys. Chem. 100 (1996) 12674–12679.
[10] M.J. Frisch, G.W. Trucks, H.B. Schlegal, G.E. Scuseria, M.A. Robb, J.R. Cheesman, V.G. Zakrzewski, J.A. Montgomerg, Jr., R.E. Strtmann, J.C. Burant, S. Dapprich, J. M. Milliam, A.D. Daniels, K.N. Kudin, M.C. Strain, O. Farkas, J. Tomasi, V. Barone, M. Cossi, R. Camme, B. Mennucci, C. Pomelli, C. Adamo, S. Clifford, J. Ochterski, G.A. Petersson, P.Y. Ayala, Q. Cui, K. Morokuma, N. Rega, P. Salvador, J.J. Dannenberg, D.K. Malich, A.D. Rabuck, K. Raghavachari, J.B. Foresman, J. Cioslowski, J.V. Ortiz, A.G. Baboul, B.B. Stetanov, G. Liu, A. Liashenko, P. Piskorz, I. Komaromi, R. Gomperts, R.L. Martin, D.J. Fox, T. Keith, M.A. Al-Laham, C.Y. Peng, A. Nsnsyskkara, M. Challacombe, P.M.W. Gill, B. Johnson, W. Chen, M.W.

Wong, J.L. Andres, C. Gonzalez, M. Head-Gordon, E.S. Replogle, J.A. Pople, GAUSSIAN 09, Revision A.02, Gaussian, Inc, Pittsburgh, PA, 2009.
[11] V. Krishnakumar, R. John Xavier, Indian J. Pure Appl. Phys. 41 (2003) 95–98.
[12] R.L. Peesole, L.D. Shield, I.C. Mcwillam, Modern Methods of Chemical Analysis, Wiley, New York, 1976.
[13] G. Socrates, Infrared and Raman Characteristic group frequencies, third ed., Wiley, New York, 2001.
[14] N.P.G. Roeges, A Guide to the Complete Interpretation of Infrared Spectra of Organic Structures, John Wiley and Sons Inc., New York, 1994.
[15] N.B. Colthup, L.H. Daly, S.E. Wiberly, Introduction to IR and Raman Spectroscopy, Academic Press, New York, 1990.
[16] H.T. Varghese, C.Y. Paniker, K.M. Pillai, Y.S. Mary, K. Raju, T.K. Manojkumar, A. Bielenica, C. Van Alsenoy, Spectrochim. Acta 76 (2010) 513–522.
[17] W.J. Balfour, Spectrochim. Acta A 39 (1983) 795–800.
[18] B. Vekkatram Reddy, G. Ramana Rao, Vib. Spectrosc. 6 (1994) 231–250.
[19] V. Ashok Babu, B. Lakshmaiah, K. Sree Ramulu, G. Ramana Rao, Indian J. Pure Appl. Phys 25 (1987) 58.
[20] N.L. Owen R.E. Hester Spectrochim. Acta 25A (1969) 343 354.
[21] G. Varsanyi vibrational spectra of Benzene derivatives 1969 Academic Press New York.
[22] R.S. Mulliken, J. Chem. Phys. 23 (1833) (1955) 2338.
[23] F.D. Angelis, S. Fntacci, A. Selloni, Nanotechnology 19 (42) (2008), 424002.
[24] E. Scrocco, J. Tomasi, Adv. Quantum Chem. 11 (1979) 115–121.
[25] Silva MAVR; LMPF, Amaral, JRB, Gomes, J. Phys. Chem. B 111 (45) (2007) 13033–13040.
[26] M. Karimi, Comput. Chem. 04 (2012) 11–16.
[27] E. AlShamaileh, Comput. Chem. 02 (2014) 43–49.
[28] M.C. Gupta, Atomic and Molecular Spectroscopy, Publishers, New Delhi, New Age International Private Limited, 2001.
[29] A. Rauk, Orbital interaction Theory of Organic Chemistry, 2nd Edition, John wiley & Sons, New York, 2001, p. 34.
[30] R.G. Parr, W. Yang, Density functional Theory of Atoms and Molecules, Oxford University Press, New York, 1989.
[31] N.M. O'Boyle, A.L. Tenderholt, K.M. Langner, cclib: A library for package-independent Computational chemistry algorithms, J. Comput. Chem. 29 (2008) 839–845.
[32] R.G. Parr, R.A. Donnelly, M. Levy, W.E. Palke, J. Chem. Phys. 69 (1978) 3801hild:: *[last()])">.
[33] R.G. Parr, R.G. Pearson, J. Am. Chem. Soc. 105 (1983) 1503.
[34] C.G. Zhan, J.A. Nichols, D.A. Dixon, J. Phys. Chem A 107 (20) (2003) 4184–4195.
[35] G. Zhang, C.B. Musgrave, J. Phys. Chem. A 111 (8) (2007) 1554–1561.
[36] Obi-Egbedi N O, Obot I B, EI-Khaiary M I, Umoren S A and Ebenso E E, (2011) Int. J. Electro. Chem. Sci., 5649-5675.
[37] R.G. Parr, L. Szentpaly, S. Liu, J. Am. Chem. Soc. 121 (1999) 1922–1924.
[38] I.B. Obot, N.O. Obi-Egbedi, S.A. Umoren, Int. J. Electchem Sci. 4 (2009) 863–877.
[39] I. Fleming Frontier Orbitals and Organic Chemical Reactions, (John Wiley and Sons 1976 New York.
[40] T. Chakraborty, D.C. Ghosh, Mol. Phys. 108 (16) (2010) 2081–2092.
[41] H. Wang, X. Wang, H. Wang, L. Wang, A. Liu, J. Mol. Model. 13 (2007) 147–153.
[42] Takao Tsuneda, Density Functional Theory in Quantum Chemistry, Springer, Japan, 2014.
[43] C. Morell, A. Grand, A. Toro-Labbe, J. Phys. Chem. 205–12 (2005).
[44] D.J. Williams, Nonlinear optical properties of organic and polymeric materials, ACS Sympos. Series 233 (1983).
[45] G.U. Bublitz, R. Ortiz, S.R. Marder, S.G. Boxer, J. Am. Chem. Soc. 119 (1997) 3365.
[46] Y.X. Zhang, F. Castet, B. Champagne, Chem. Phys. Lett. (2013) 57442–57446.
[47] B.J. Coe, J. Fielden, S.P. Foxon, J.A. Harris, M. Helliwell, B.S. Brunschwig, C. K. Asselberghs, J. Garın, J. Orduna, J. Am. Chem. Soc. 132 (2010) 10498–10512.
[48] M. Karabacak, M. Kurt, M. Cinar, S. Ayyappan, S. Sudha, N. Sundraganesan, Spectrochim. Acta Part A 92 (2012) 365–376.
[49] M.R.S.A. Janjua, M.U. Khan, B. Bashir, M.A. Iqbal, Y.Z. Song, S.A.R. Naqvi, Z. A. Khan, Comput. Theor. Chem. 994 (2012) 34–40.
[50] Y.L. Si, G.C. Yang, J. Mater. Chem. C 1 (2013) 2354–2361.
[51] M. Grätzwl, Recent Advances in sensitized mesoscopic solar cells, Acc. Chem. Res. 42 (2009) 1788–1798.
[52] A. Gadisa, M. Svensson, M.R. Andersson, O. Inganas, Appl. Phys. Lett. 84 (2004) 1609.
[53] J. Preat, C. Michaux, D. Jacquemin, E.A. Perpete, J. Phys. Chem. C 113 (2009) 16821–16824.
[54] J.B. Asbury, Y.Q. Wang, E. Hao, H.N. Ghosh, T. Lian, Res. Chem. Intermed. 27 (2001) 393–406.

[55] R. Katoh, A. Furube, T. Yoshihara, K. Hara, G. Fujihashi, S. Takano, S. Murata, H. Arakwa, M. Tachiya, J. Phys. Chem. B 108 (2004) 4818–4822.

[56] A. Islam, H. Sugihara, H. Arakawa, J. Photochem. Photobiol. A 158 (2003) 131–138.

[57] T. Daeneke, A.J. Mozer, Y. Uemura, S. Makuta, M. Fekete, Y. Tachiibana, N. Koumura, U. Bach, L. Spiccia, J. Am. Chem. Soc. 134 (2012) 16925–16928.